Electrodic voltages accompanying stimulated bioremediation of a uranium-contaminated aquifer

Kenneth H. Williams[1], A. Lucie N'Guessan[2], Jennifer Druhan[3], Philip E. Long[2], Susan S. Hubbard[1], Derek R. Lovley[4], and Jillian F. Banfield[3]*

[1]Lawrence Berkeley National Laboratory, Berkeley, CA 94720

[2]Pacific Northwest National Laboratory, Richland, WA 99352

[3]Dept. of Earth and Planetary Science, University of California, Berkeley, CA 94720

[5]Dept. of Microbiology, University of Massachusetts, Amherst, MA 01003

[*]**Corresponding author**: Kenneth H. Williams; phone: 510.701.1089

Email addresses: khwilliams@lbl.gov, lucie.nguessan@pnl.gov, jennydruhan@berkeley.edu, philip.long@pnl.gov, sshubbard@lbl.gov, dlovley@microbio.umass.edu, jbanfield@berkeley.edu

Abstract

The inability to track the products of subsurface microbial activity during stimulated bioremediation has limited its implementation. We used spatiotemporal changes in electrodic potentials (EP) to track the onset and persistence of stimulated sulfate-reducing bacteria (SRB) in a uranium-contaminated aquifer undergoing acetate amendment. Following acetate injection, anomalous voltages approaching -900 mV were measured between copper electrodes within the aquifer sediments and a single reference electrode at the ground surface. Onset of EP anomalies correlated in time with both the accumulation of dissolved sulfide and the removal of uranium from groundwater. The anomalies persisted for 45 days after halting acetate injection. Current-voltage and current-power relationships between measurement and reference electrodes exhibited a galvanic response, with a maximum power density of 10 mW/m^2 during sulfate-reduction. We infer that the EP anomalies resulted from electrochemical differences between geochemically reduced regions and areas having higher oxidation potential. Following the period of sulfate reduction, EP values ranged from -500 to -600 mV and were associated with elevated concentrations of ferrous iron. Within 10 days of the voltage decrease, uranium concentrations rebounded from 0.2 to 0.8 μM, a level still below the background value of 1.5 μM. These findings demonstrate that EP measurements provide an inexpensive and minimally invasive means for monitoring the products of stimulated microbial activity within aquifer sediments and are capable of verifying maintenance of redox conditions favorable for the stability of bioreduced contaminants, such as uranium.

Introduction

Radionuclide contamination of groundwater is an ongoing problem at many former uranium ore-processing sites under the control of the U.S. Department of Energy. Continued leaching of residual uranium at such sites has resulted in low-level but persistent contamination of both groundwater and sediments within local aquifers. Research efforts are currently underway to promote the *in situ* removal of soluble U(VI) species via stimulated bioremediation at the Rifle Integrated Field Research Challenge (IFRC) site near Rifle, Colorado (Figure 1), the site of a former mill tailings facility. Repeated biostimulation experiments at the site [*Anderson et al.* , 2003; *Vrionis et al.* , 2005] have shown that acetate injection into the aquifer promotes the growth of dissimilatory metal-reducing bacteria of the family *Geobacteraceae* and a decline in the U(VI) content of groundwater downgradient from the injection site. The reproducible, stimulated growth of *Geobacteraceae* along with the correlated loss of U(VI) suggests that these organisms are responsible for the *in situ* reduction of U(VI), a fact corroborated by both laboratory [*Finneran et al.*, 2002; *Holmes et al.*, 2002; *Ortiz-Bernad et al.*, 2004] and field studies [*Senko et al.* , 2002; *North et al.* , 2004; *Peacock et al.* , 2004; *Ginder-Vogel et al.*, 2005; *Wu et al.*, 2006].

Prolonged addition of acetate to the aquifer results in a shift in the dominant terminal electron-accepting pathway from iron- to sulfate-reduction. This is evidenced by groundwater and sediment samples enriched in members of the order *Desulfobacterales* [*Vrionis et al.*, 2005] and a decrease in ferrous iron and sulfate within the aquifer. An unintended consequence of this shift in metabolism is an initial decrease in the rate of removal of soluble U(VI) from groundwater [*Anderson et al.* , 2003]. At

longer time points, however, and upon cessation of acetate injection, sustained removal of U(VI) under conditions of sulfate-reduction does occur, ultimately reaching levels comparable to those achieved during the initial period of iron-reduction.

While the process of U(VI) removal both during and after the period of sulfate-reduction is still under investigation, it is believed to result from a variety of causes, including reductive immobilization of U(VI) by non-acetate oxidizing sulfate-reducers and sorption onto a combination of cell surfaces [*N'Guessan et al.* , 2008] and altered mineral phases [*Catalano and Brown*, 2005]. While these results suggest the importance of maintaining conditions of iron-reduction for optimizing the reductive immobilization of U(VI), the sustained removal of U(VI) during and after stimulated sulfate-reduction indicates that its onset is not completely undesirable, especially under geochemical conditions (i.e. high sulfate) where it is likely to be an unavoidable outcome of organic carbon amendment. Furthermore, the production of redox-poising constituents accompanying stimulated sulfate-reduction (e.g. FeS, reduced phyllosilicates, and H_2S) may offer a means for prolonging the stability of insoluble, bioreduced phases, such as UO_2.

There is growing interest in the use of geophysical methods to better inform the decision-making process during environmental remediation activities. The inherent variability in rapidly delineating subsurface transformations accompanying remediation activities, such as those that occur during stimulated bioremediation, often limit the speed with which the remediation approach may be modified to improve its success. Among such methods, the self-potential (SP) technique has shown promise as an inexpensive yet sensitive means for delineating variations in subsurface geochemical conditions resulting

from biological processes [*Nyquist and Corry* , 2002; *Naudet et al.* , 2003; *Naudet and Revil*, 2005; *Arora et al.*, 2007]. The SP method is a passive technique that measures the open-circuit voltage potential between electrodes located at the ground surface or within boreholes, with the potential-generating mechanism varying according to environmental and measurement conditions [*Sato and Mooney* , 1960; *Corry*, 1985; *Bigalke and Grabner*, 1997; *Nyquist and Corry*, 2002; *Cameron et al.*, 2004; *Minsley et al.*, 2007].

Under conditions where the measurement and reference electrodes are (a) located in geochemically distinct redox environments and (b) exposed to their local geochemical environment, a subset of the SP method - referred to as the electrodic potential (EP) method - has been shown to be sensitive to electrochemical reactions involving the electrodes themselves [*Corry*, 1985; *Nyquist and Corry* , 2002; *Williams et al.* , 2007; *Slater et al.*, 2008]. When bridged through a measuring voltmeter, electrodes located in the electrochemically distinct regions constitute a galvanic cell, generating a voltage potential that persists as long as the concentration gradient is maintained. Under conditions that lead to the spontaneous flow of current when the two electrodes are connected, electrons flow from the anode during an oxidation reaction to the cathode in a coupled reduction reaction. Charge balance is maintained via electrolytic conduction through the pore space, which also acts to complete the overall circuit. Under conditions where the geochemical environment directly interacts with the electrode surface (e.g. during a corrosive process), the electrode composition will determine the nature of the measured half-cell reaction. The magnitude of the anomalous open-circuit potentials may be quantitatively interpreted in the same manner as voltages that result when using an ion-selective electrode, albeit over a scale of meters rather than millimeters.

The galvanic mechanism underlying the EP response (Figure 2) may be illustrated using the electrode pair in which the measurement and reference electrodes are composed of Cu^0 and $Cu^0/CuSO_4$, respectively, with the latter being a non-polarizing electrode design frequently used for SP measurements. When a reduced electroactive species (e.g. bisulfide or HS^-) is present near the measurement electrode and the reference electrode is maintained in a more oxidized environment, a sulfide-dependent voltage potential of 700-900 mV will result from the coupling of the two half-cell reactions: the oxidation of Cu^0 (as CuS or Cu_2S) at the measurement electrode (i.e. the anode) and the reduction of $CuSO_4$ (as Cu^0) at the reference electrode (i.e. the cathode). Because of the high input impedance of the voltmeter (>10 MΩ), there is negligible transfer of electrons during the measurement process and consumption of electro-active species is insignificant. For anodic reactions that are both thermodynamically and kinetically favorable, such as those occurring between dissolved sulfide and base metals, such a galvanic response will dominate the measured EP signal.

In the absence of HS^-, anomalous EP voltages may still be the result of a galvanic effect where the measurement electrode acts as a non-reactive surface sensitive to the dominant electrochemical half-cell reaction in its vicinity. In such a configuration, the measurement electrode serves the same function as the platinum electrode in an oxidation-reduction potential (ORP) probe. The mechanism is relevant in the presence of aqueous ferrous iron, the byproduct of microbial iron reduction. A ferrous iron dependent voltage potential of 550-700 mV will result from the coupling of the two half-cell reactions: oxidation of Fe^{2+} at the measurement electrode surface and the reduction of $CuSO_4$ (as Cu^0) at the reference electrode.

Interpreting the electrodic response within the context of a galvanic model makes it possible to use temporal EP anomalies to monitor geochemical changes induced by the stimulation of microbial activity. Here we show that the appearance and persistence of dissolved sulfide correlates with the generation of significant EP voltage anomalies indicative of subsurface microbial sulfate-reduction. Furthermore, spatiotemporal variations in the onset and sustenance of the EP anomalies appear to track the location of active metabolism within the aquifer, offering an indirect means for verifying geochemically reduced conditions conducive to the removal of aqueous uranium. By interpreting such potentials within the context of predictable and quantifiable galvanic reactions, the EP monitoring approach offers a sensitive, inexpensive and minimally invasive means for detecting the presence of metabolic end products, such as dissolved sulfide and ferrous iron.

Materials and Methods

Site Description and Experimental Approach

A comprehensive description of the local geology, hydrology and geochemistry of the Rifle IFRC site, as well as the general methodological approach to acetate injection, has been presented elsewhere [*Anderson et al.*, 2003; *Vrionis et al.*, 2005; *Yabusaki et al.*, 2007]. Briefly, the site is located on a flood plain, ~9.0 hectares in area, in Northwestern Colorado (Figure 1). The local aquifer is comprised of an unconsolidated mixture of alluvial sands, silts, clays and gravels deposited by the adjacent Colorado River. The aquifer thickness is ca. 6.5 m, with the saturated interval occurring at a depth of approximately 3.5 to 4.0 m below ground surface (bgs). The hydrology of the site is

characterized by relatively high groundwater velocities (~0.30 m day^{-1}) and a water table that varies according to river stage, rising by as much as 1.5 m during periods of peak runoff. Large variations in hydraulic conductivity exist over the saturated interval, with values ranging from 0.50 to 50 m day^{-1}. Core recovery during well installation has repeatedly identified a 0.5-0.7 m thick, high permeability sandy layer at depth of ~3.7 m bgs and spanning the water table. This unit may contribute to enhanced rates of groundwater flux during recharge events, acting as a conduit for the introduction of partially oxygenated groundwater. The site is underlain by the relatively impermeable weathered claystone of the Wasatch formation, which acts as a lower boundary to fluid flow.

Groundwater samples were obtained from a series of monitoring wells located within a test area encompassing approximately 50 square meters. A single background monitoring well was located 3.5 m upgradient from an injection gallery positioned perpendicular to groundwater flow and comprised of five boreholes spaced at 0.6 m intervals (Figure 1). Four downgradient monitoring wells were located at 1.5 m intervals, beginning at a distance of ~1.0 m from the injection gallery. Two specially designed well casings incorporating metallic copper (Cu^0) electrodes were located 2.0 m downgradient (SP-1) and 1.0 m upgradient (SP-2) from the injection gallery (Figures 2 and S1). The casing materials (PVC; 5 mm slot size) and method of completion of the two electrode wells were identical for all injection and monitoring wells. Each of the electrode-modified casings incorporated eleven bands of Cu^0 (5.7 cm diameter, 2 cm width) located at 25 cm intervals along the casing length (Figure S1). After installation, the upper- and bottommost electrodes in each well were located at 4.0 m and 6.5 m bgs, respectively.

The electrodes were attached to the outside of the well casing using copper rivets and connected to the surface via insulated wires; all connections were made water tight using an epoxy sealant. After installation, the electrodes were allowed to equilibrate for 30 days before beginning acetate injection.

Ten electrodes from each of the two wells spanning the 4.0-6.25 m bgs depth interval were connected to a high impedance, multi-channel voltmeter programmed to measure the open-circuit potential between each electrode and a surface-based reference electrode at 6-hour intervals. Continuous recording of the EP signals began 2 days prior to the onset of acetate injection. The measurement convention was such that the negative lead of the voltmeter was connected to the reference electrode and the positive lead connected to the downhole electrode. The reference consisted of a $Cu^0/CuSO_4$ non-polarizing electrode located in a shallow, tarp-covered hole in the vicinity of the southeastern most injection well; the contact resistance between the reference and each of the casing-affixed Cu^0 electrodes ranged from 500 to 900 Ω. Allowing time for equilibration, installation of the reference electrode occurred immediately after installation of the borehole electrodes. The tarp prevented excess moisture from submerging the reference electrode during rainfall events and sporadic measurements of contact resistance fell within the aforementioned range.

Current-voltage and current-power relationships were periodically determined between the bottommost electrode (6.5 m bgs) in each well and a second surface-based $Cu^0/CuSO_4$ reference electrode by measuring the voltage drop across a range of resistances from 4 MΩ to 10 Ω. A second surface-based electrode was used in order to minimize disturbance of the reference electrode resulting from current flow during the

current-voltage and current-power measurements. These measurements were made before, during (days 58 and 85), and after biostimulation (day 115). Following re-equilibration of the open-circuit electrode response, current flow between the same two electrode pairs was determined by measuring the voltage drop across a known resistance (500 Ω) for a fixed length of time (ca. 20 hours) both before and during biostimulation (day 59).

Groundwater was pumped from an upgradient portion of the aquifer into a surface storage tank and amended with sodium acetate and potassium bromide in quantities sufficient to achieve *in situ* concentrations of 10 mM and 1 mM, respectively, upon injection. Acetate-amended groundwater was introduced to the aquifer over the entire saturated thickness (18 mL/min per borehole; 3.5 to 6.5 m bgs) using a combination of peristaltic and crosswell mixing pumps to continuously cycle the injectate between the five injection wells to achieve better uniformity in the distribution of acetate during the injection phase.

Acetate was injected over a 68-day period between July and September 2006, during which time groundwater was systematically sampled at 2 to 14 day intervals from each of the monitoring wells to characterize changes in geochemical composition. While groundwater samples were obtained for each of the non-electrode monitoring wells prior to the injection of acetate, samples were not obtained from the electrode-bearing wells until 42 days after starting the injection of acetate. After this time, groundwater samples were obtained from all of the wells at regular intervals for the duration of the experiment. Both the geochemical sampling and the multi-electrode voltage logging continued for a total of 185 days, or 117 days following the cessation of acetate injection.

Groundwater was sampled from each well over the 4.1-4.4 m bgs depth interval using a peristaltic pump connected to a flow-through multi-parameter probe designed to measure dissolved oxygen, fluid conductivity, pH, and redox potential. All wells were purged until the parameters stabilized (ca. 12 L; 0.5 L min^{-1}), after which time the probe was disconnected and groundwater samples were taken directly from the pump outflow. All samples were filtered with 0.2 μm-pore-size syringe filters before preservation. Samples designated for U(VI) and SO_4^{2-} analysis were placed into sterile, no-headspace 15 mL tubes, while those designated for acetate analysis (19 mL) were placed into no-headspace glass containers and preserved with 1 mL of 0.1 M H_2SO_4. These samples were returned via overnight courier to the laboratory and stored at 4°C prior to analysis. Ferrous iron and sulfide analyses were performed immediately upon sampling, with the samples diluted, as needed, using de-ionized water.

Uranium was measured by kinetic phosphorescence analysis as previously described [*Finneran et al.* , 2002]. Acetate was measured with high-pressure liquid chromatography using a fast-acid analysis column with an 8 mM H_2SO_4 eluent and absorbance detection (210 nm). Sulfate was determined via ion chromatography using an AS4A-SC analytical column with a carbonate/bicarbonate eluent (1.8 mM/1.7 mM). Ferrous iron and sulfide concentrations were determined colorimetrically by previously described techniques [*Cline*, 1969; *Lovley and Phillips*, 1987].

Results

Impact of Acetate Injection on Electrodic Potential Response

During the 30-day equilibration period prior to acetate injection, the open-circuit potentials reached quasi-steady state values ranging from -310 to -440 mV. The range of baseline voltages is likely due to variability in the immediate geochemical conditions surrounding each electrode and the extent to which each electrode was electrically coupled to the sediments. Following the injection of acetate, a pronounced increase in voltage magnitude was observed for both wells at all electrode locations (Figures 3 and 4). As a result of the measurement convention, the anomalous EP effect is reported as an increase in voltage magnitude, with values becoming more negative with time (e.g. -400 mV to -900 mV).

In the case of the downgradient electrode well (SP-1), increases in voltage magnitude from pre-injection values were observed for all electrode locations within the first 20-25 days (Figure 3). Across the depth interval, there was considerable variability in the time it took to reach the most negative EP values. In general, the shallower electrode locations, and in particular, the locations closest to the water table, exhibited the longest lag times before reaching their most negative value. Upon reaching values between -850 and -900 mV, the EP values fluctuated within the range from -740 to -900 mV throughout the period of acetate injection.

Although injection of acetate into the aquifer was halted after 68 days, EP values more negative than -800 mV persisted for an additional 50 days (Figure 3). The length of time that such voltages persisted generally increased with depth. After a total elapsed time of 115 days, or 47 days after acetate injection was halted, EP values across the entire measurement interval approached relatively uniform levels of -550±40 mV.

Electrodes located upgradient from the injection gallery never yielded EP anomalies in excess of -810 mV. Shortly after beginning the acetate injection, voltages along the length of SP-2 reached relatively stable values of -650±25 mV (Figure 4). Voltages remained within this range for the duration of the injection period, except for a few electrode locations where EP values approached -800 mV over the final 5-7 days of the injection period. Immediately following cessation of acetate addition, EP values rebounded to levels of -500 to -550 mV remaining relatively constant for the duration of the experiment.

Direct comparison of the temporal voltage response for a discrete electrode location in each well (5.0 m bgs) reveals several interesting features (Figure S2). Although the onset of the EP anomalies occurs at a similar time following the injection of acetate, the persistence of the anomalies and their absolute magnitude is distinct for both locations. Following the first 20-days, voltages in SP-2 reach a relatively stable value of -670 mV, while the values recorded in SP-1 continue to decrease for another 8-days, reaching a value of -840 mV by day 28. Subsequently, the voltages in both wells fluctuated within a narrow range before transitioning to relatively stable, post-amendment levels. The transition was delayed in SP-1 relative to SP-2 by 31 days.

Current-voltage and current-power relationships were determined for each EP monitoring well before, during, and after acetate injection. While there was negligible current flow between the measurement and reference electrodes prior to starting acetate injection (data not shown), when measured 58- and 85-days into the experiment, current- and power-densities for both electrode pairs were significantly elevated above baseline (Figure 5). Following the post-injection rebound in EP values, current- and power-

densities decreased for both wells by up to one order of magnitude after 150-days, returning to levels similar to, but slightly elevated above, pre-injection values.

Current flow from the deepest electrode location in SP-1 (6.5 m bgs) to the surface electrode increased approximately four orders of magnitude with a concomitant forty-fold decrease in voltage over the resistance range measured (Fig. 5). When normalized to the surface area of the measurement electrode (50 cm^2), the resulting current density over this resistance range increased from 0.004 to 46 $\mu A/cm^2$. Power densities between the electrodes showed a parabolic trend reaching a maximum value of 9.7 $\mu W/cm^2$ at 400 Ω. Similar values were observed for the same electrode pair 85-days after acetate injection began. This was not the case following the cessation of acetate injection. By day 150, both current- and power-density decreased dramatically, reaching maximum values of 2.4 $\mu A/cm^2$ and 0.305 $\mu W/cm^2$, respectively. Identical measurements made between SP-2 and the surface electrode revealed a similar trend, with anomalously high current flow and power production during acetate injection. Only the results from the measurements made on day 58 are presented (Figure 5).

Power production from SP-1 (6.5 m bgs) to the surface reference electrode was measured over two ~20-hour time windows, once before and again 59-days after commencing acetate injection (Figure S3). Prior to injection, power densities remained relatively constant at ~0.018 $\mu W/cm^2$ over the measurement period. Following acetate-injection, current flow increased by approximately two orders of magnitude. Power density decreased rapidly over the first 1.5-hours of measurement, reaching a quasi-steady state value of 1.0±0.15 $\mu W/cm^2$ for the remaining 18-hour recording interval.

Impact of Acetate Injection on Aquifer Geochemistry

Prior to the injection of acetate, the geochemical composition of the groundwater was fairly consistent across the experimental plot, having very low dissolved oxygen (<6 μM), circumneutral pH (ca. 7), relatively high specific conductivity (ca. 2400 μS cm^{-1}), and SO_4^{2-} and U(VI) concentrations ranging from 7.2±0.2 mM, and 1.5±0.1 μM, respectively. Background concentrations of ferrous iron (Fe^{2+}) showed greater variability, ranging from 4.5 μM in the upgradient well to 3.5-45 μM in the downgradient wells.

Following the injection of acetate, geochemical conditions downgradient from the injection gallery changed rapidly. Acetate and bromide (data not shown) were detected in the downgradient wells within 3-days. Both species remained at detectable levels for the duration of the 68-day injection period, with acetate not falling to levels below detection until 16-days after injection was suspended. The concentration of sulfide in the downgradient wells rose rapidly after day 15, fluctuating somewhat, but remaining elevated for the duration of the injection period and beyond (Figure 6A). A significant decrease in redox potential (Figure 6B) accompanied the accumulation of sulfide, as did an increase in pH (Figure 6C). Neither geochemical indicator returned to baseline levels until significant depletion of sulfide occurred approximately 24 days after acetate injection ceased. Subsequently, downgradient concentrations of Fe^{2+} increased steadily over the remainder of the experimental period, whereas upgradient concentrations remained unchanged or decreased somewhat over the same interval. The rebound in EP values observed in both electrode wells after halting acetate injection closely tracked the transition from a sulfide-dominated system to one characterized by elevated concentrations of Fe^{2+} (Figure S4). Overall an excellent temporal correlation was found

to exist between the downgradient EP response and the sulfide and ferrous iron concentrations, E_h, and pH values observed in M-21.

As expected given its upgradient location, sulfide concentrations in SP-2 were typically below detection over the same sampling period (data not shown). Sulfide concentrations measured in SP-1 after day 42 were similar to concentrations in the other downgradient wells, although higher levels were occasionally detected (Figure S5). The accumulation of sulfide in the downgradient wells was always accompanied by a concomitant decrease in sulfate (data not shown), levels of which did not return to background values until 30-days after acetate injection ceased.

Dissolved uranium concentrations began to decrease downgradient of the injection gallery within 5 days after starting acetate injection (Figure S6). Uranium concentrations decreased to their lowest level after 27 days, after which time they rebounded somewhat for the duration of the injection. The initial decrease coincided with the accumulation of Fe^{2+} and extended into the period of sulfide accumulation. The rebound in uranium closely tracked the rapid increase in pH (Figure 6C) and the near complete removal of sulfate (data not shown). Following the end of acetate injection, uranium concentrations fell to their lowest levels, with a high degree of removal occurring for another 50 days. EP values in excess of -800 mV correlated generally with high rates of uranium removal over the entire experimental period and strongly in the period following the cessation of acetate injection. Once EP values fell below -650 mV, significant removal of uranium continued for a period of less than 15 days.

Galvanic Assessment of Self-Potential Signals

Laboratory EP measurements were made using a galvanic cell to explore the mechanism underlying the anomalous voltages observed during sulfate-reduction. As sulfide concentrations within the anodic chamber were increased from 0.004 to 4 mM, the absolute value of the EP voltage measured between the cathodic reference electrode ($Cu^0/CuSO_4$; 1 M $CuSO_4$) and anodic measurement electrode (Cu^0) increased from 120 to 938 mV, respectively (Figure 7). A strong correlation existed between the EP values and the sulfide-mediated cell potentials for concentrations in excess of 0.01 mM. Below this concentration, the theoretical cell potentials significantly over-predicted the measured EP response, in agreement with previous findings [*Williams et al.* , 2007]. Current-voltage and current-power relationships using the 1 mM concentration confirmed the transfer of electrons from anode to cathode upon completion of the circuit, with the results (data not shown) closely matching those obtained on day 58 of the field experiment.

Discussion

To validate the galvanic interpretation of the EP response [*Corry*, 1985; *Nyquist and Corry* , 2002], we showed that under certain laboratory conditions and electrode configurations EP anomalies reflect geochemical concentration gradients and yield voltages predictable from the coupled half-cell reactions [*Williams et al.*, 2007]. Here we tested the hypothesis that electrodic voltages measured between inexpensive and robust copper electrodes could be used to monitor the geochemical evolution of a uranium-contaminated aquifer undergoing stimulated bioremediation. Our results confirm that electrochemical interactions between an electrode surface and the surrounding environment over spatial scales exceeding 10 meters can generate significant EP

anomalies. We attribute the anomalies to electrochemical concentration gradients that developed between both sulfide- and Fe^{2+}-rich regions and areas having higher oxidation potential (e.g., the ground surface). Temporal voltage variations were diagnostic of the dominant metabolic process during and after acetate amendment and exhibited a general correlation with enhanced rates of uranium removal.

Evidence in support of a galvanic mechanism underlying the EP response comes from the power production results. We observed significant electron flow through the circuit created by connection of the measurement and reference electrodes. Current- and power-densities are in excellent agreement with those reported for sulfide-dependent galvanic fuel cells [*Tender et al.*, 2002; *Rabaey et al.*, 2006; *Reimers et al.*, 2006]. If the transfer of electrons from reduced to oxidized locations via an endogenous conductor had been the dominant source of the measured potentials, current flow through the circuit would have been negligible. The EP signals are therefore unlikely to have resulted from electron transfer through biogenic materials [*Naudet et al.*, 2003; *Naudet and Revil*, 2005; *Reguera et al.*, 2005; *Reguera et al.*, 2006; *Ntarlagiannis et al.*, 2007] or mineral phases [*Sato and Mooney* , 1960] and anomalies of the magnitude reported here cannot be generated via electrochemical diffusion driven by chemical concentration gradients [*Nourbehecht*, 1963].

When the measurement and reference electrodes were bridged through a voltmeter, a spontaneous galvanic cell was created, with the intervening saturated sediments acting as the salt bridge necessary for charge conservation and completion of the circuit (Figure 2). Oxidation of Cu^0 to either CuS or Cu_2S at the measurement electrode (anode) occurred during periods of sulfate-reduction, coupled to the reduction

of Cu^{2+} to Cu^0 at the reference (cathode). Under conditions where Fe^{2+} was the dominant species, the oxidation of ferrous to ferric iron at the measurement electrode was coupled to the aforementioned cathodic reaction.

In considering the anodic half-cell reactions, the geochemical species mediating the galvanic reactions may either be reactive or passive with respect to the electrode surface. In the case of the former, bisulfide (the dominant aqueous sulfide phase at pH ≥7) can react directly with the copper measurement electrode:

$$CuS_{(s)} + H^+ + 2e^- \rightarrow Cu^0{}_{(s)} + HS^-{}_{(aq)} \qquad E^0 = -0.338 \text{ V} \qquad (1)$$

$$Cu_2S_{(s)} + H^+ + 2e^- \rightarrow 2Cu^0{}_{(s)} + HS^-{}_{(aq)} \qquad E^0 = -0.516 \text{ V} \qquad (2)$$

where the copper sulfide phase favored (CuS or Cu_2S) depends upon the sulfide concentration and the specific pH and E_h conditions surrounding the electrode (Figure S7). Under persistent sulfidic conditions, variations in these three parameters yield potentials that can vary over a range of nearly 180 mV.

Under conditions where Fe^{2+} is the dominant aqueous species in proximity to the electrode, the measurement electrode surface is inert and serves the same function as the platinum electrode in an ORP probe:

$$FeOOH_{(s)} + 3H^+ + 1e^- \rightarrow Fe^{2+}{}_{(aq)} + 2H_2O \qquad E^0 = 0.661 \text{ V} \qquad (3)$$

where the form of the iron oxide (here, goethite) determines the value of the reduction potential. Mineralogical analysis of aquifer sediments from the Old Rifle site has identified goethite as a dominant oxide phase, and its inclusion in (3) yields cell potentials in excellent agreement with the EP values observed under Fe^{2+}-rich conditions (Figure S8).

In the absence of competing reactions, the cathodic half-cell reaction is simply that of the standard $Cu^0/CuSO_4$ reference electrode, here written as a reduction reaction:

$$Cu^{2+} + 2e^- \rightarrow Cu^0_{(s)} \qquad E^0 = 0.340 \text{ V} \qquad (4)$$

With the measurement and reference electrodes thus configured, the reduction potentials for the coupled half-cell reactions may be calculated, corrected for concentration-specific effects using the Nernst equation, and subtracted to yield the overall cell potential for the galvanic pair.

Laboratory experiments in which sulfide concentration gradients were systematically varied showed a positive correlation between the magnitude of the measured EP anomaly and the theoretical cell potentials (Figure 7), particularly for sulfide concentrations in excess of 10 μM. Given the sulfide concentrations observed during the field biostimulation experiment (30-600 μM), equations (1) and (2) yield theoretical cell potentials of 740-970 mV, respectively, in close agreement with the observed EP anomalies. Consequently, the EP anomalies may be used as a semi-quantitative means for assessing redox zonation under field conditions, especially as it pertains to the activity of sulfate-reducing microorganisms.

Hydrogeological variability influences the pattern of acetate delivery, thereby controlling the onset of sulfate-reduction within the Rifle aquifer. The initial accumulation and subsequent dispersal of sulfide can be documented using the temporal EP response. In general, the deeper electrodes responded more rapidly than the shallower electrodes. Furthermore, EP values for locations closer to the water table rebounded faster than deeper locations after acetate addition ceased. The high permeability sandy layer straddling the water table may provide a conduit for re-oxygenation of groundwater, inhibiting the onset of sulfate-reduction and limiting its persistence at shallower as compared to deeper locations in the aquifer. These results indicate the utility of EP measurements for assessing the impact of vertical heterogeneity on remediation efficacy – an important criterion when implementing remediation approaches across large spatial scales.

The EP monitoring results suggest eventual delivery of nutrients throughout the saturated profile downgradient of the injection gallery, an important criterion for bioremediation success at this site [*Vrionis et al.*, 2005]. The strong depth dependence of the onset of sulfide production in downgradient locations, as indicated by the vertical stratification in EP values (Figure 3), indicates that growth of sulfate-reducing bacteria exclusively within the wellbore is not the primary source of the EP response. Geochemical stratification within the borehole should be rapidly eliminated by diffusion and direct mixing resulting from weekly pumping of 5 to 7 L purge volume during fluid sampling.

As shown in Figures 3, 6 and S2, the temporal electrode response during the period of active sulfate-reduction varied within the 178 mV range bracketed by the CuS-

and Cu_2S-forming reactions. Voltage fluctuations within these bounds are expected and diagnostic of sulfate-reduction, and they need not be ascribed to an erratic electrode response that yields noisy or questionable data. As shown in Figure S7, expansion of the stability field of CuS occurs as sulfide concentrations increase. Consequently, EP values indicative of CuS rather than Cu_2S formation may be diagnostic of higher sulfide concentrations in proximity to the electrode surface. However, changes in pH and E_h also alter the stability of the two copper sulfide phases.

It is important to note that sustained uranium removal corresponded to EP values in excess of -800 mV, reflective of geochemical conditions favorable to the stability of the Cu_2S, rather than the CuS couple. Fluctuations of EP anomalies toward conditions conducive to the stability of CuS correlate with higher aqueous uranium concentrations in the downgradient wells. This may result from either the remobilization of formerly sequestered uranium or reduced rates of uranium removal. Regardless, geochemical conditions that yield EP anomalies more negative than -800 mV appear to offer a diagnostic means for assessing conditions favorable for the sustained immobilization of uranium.

The predicted potentials when coupling the anodic oxidation of Fe^{2+} at the measurement electrode to the cathodic reduction of Cu^{2+} at the reference electrode for a range of Fe^{2+} concentrations are shown in Figure S8. The abrupt transition in downgradient EP values following termination of sulfate-reduction correlates with the steady increase in Fe^{2+} above background levels (Figure S4). Measured Fe^{2+} concentrations correspond to those estimated from EP data (Figure S8). While the mechanism of Fe^{2+} generation was not confirmed, the post-injection increase in Fe^{2+} in

the downgradient wells is inferred to result from residual microbial iron-reduction, the subsequent release of Fe^{2+} following the oxidation of FeS precipitated during sulfate-reduction, or both. The steady decrease in EP magnitude for the downgradient locations even under conditions where Fe^{2+} concentrations increase from 10 to 40 μM is explained via the galvanic model when the predicted cell potentials are corrected for the temperature decrease from 17 to 10ºC observed during geochemical sampling (Figure S8).

Conclusions

Our results show the potential of using galvanic techniques for efficiently monitoring regions of stimulated bioremediation, an emerging approach for sequestration of toxic metals and radionuclides. Specifically, we have shown that the accumulation of metabolic end products near an electrode surface during biostimulation creates electrochemical changes that are directly detectable using the electrodic potential method under field conditions. We have resolved spatiotemporal changes in open-circuit potentials resulting from variations in the onset, location, and sustenance of sulfate reduction, as well as those resulting from the accumulation of Fe^{2+} associated with iron reduction or its release accompanying FeS oxidation. EP measurements using robust, inexpensive, and widely deployable metallic electrodes may thus be useful for evaluating the sustenance of redox conditions favorable for the long-term stability of reduced precipitates, better enabling the post-closure management of contaminated sites.

Acknowledgments. Funding was provided by the Environmental Remediation Science Program, Office of Biological and Environmental Research, U.S. Department of Energy (DE-AC02-05CH1123 to LBNL; cooperative agreement DE-FC02ER63446 to PNNL). We thank Dr. Qusheng Jin (University of Oregon) for his assistance with constructing the Eh-pH diagram for the Cu-S-O system.

This document contains auxiliary/supporting information consisting of eight figures intended to supplement the material presented in the manuscript. These include a photograph of the electrode-affixed well casings, co-plots of electrodic potential and geochemical data, an Eh-pH diagram for the Cu-S-O system, current-voltage/current-power relationships, and theoretical cell potentials for the Fe(II)/FeOOH||Cu(II)/Cu system.

References

Anderson, R. T., H. A. Vrionis, I. Ortiz-Bernad, C. T. Resch, P. E. Long, R. Dayvault, K. Karp, S. Marutzky, D. R. Metzler, A. Peacock, D. C. White, M. Lowe, and D. R. Lovley (2003), Stimulating the in situ activity of Geobacter species to remove uranium from the groundwater of a uranium-contaminated aquifer, *Appl. Environ. Microb.*, *69*(10), 5884-5891.

Arora, T., N. Linde, A. Revil, and J. Castermant (2007), Non-intrusive characterization of the redox potential of landfill leachate plumes from self-potential data, *J. Contam. Hydrol.*, *92*(3-4), 274-292.

Bigalke, J., and E. W. Grabner (1997), The Geobattery model: a contribution to large scale electrochemistry, *Electrochim. Acta*, *42*(23-24), 3443-3452.

Cameron, E. M., S. M. Hamilton, M. I. Leybourne, G. E. M. Hall, and M. B. McClenaghan (2004), Finding deeply buried deposits using geochemistry, *Geochem-Explor. Env. A*, *4*, 7-32.

Catalano, J. G., and G. E. Brown (2005), Uranyl adsorption onto montmorillonite: Evaluation of binding sites and carbonate complexation, *Geochim. Cosmochim. Acta*, *69*(12), 2995-3005.

Cline, J. D. (1969), Spectrophotometric determination of hydrogen sulfide in natural waters, *Limnol. Oceanogr.*, *14*(3), 454-458.

Corry, C. E. (1985), Spontaneous Polarization Associated with Porphyry Sulfide Mineralization, *Geophysics*, *50*(6), 1020-1034.

Finneran, K. T., R. T. Anderson, K. P. Nevin, and D. R. Lovley (2002), Potential for Bioremediation of uranium-contaminated aquifers with microbial U(VI) reduction, *Soil Sediment Contam.*, *11*(3), 339-357.

Ginder-Vogel, M., W. M. Wu, B. H. Gu, J. Carley, J. Nyman, C. Criddle, P. Jardine, and S. Fendorf (2005), In-situ biological reduction of uranium within fractured saprolite, *Geochim. Cosmochim. Acta*, *69*(10), A464-A464.

Holmes, D. E., K. T. Finneran, R. A. O'Neil, and D. R. Lovley (2002), Enrichment of members of the family Geobacteraceae associated with stimulation of dissimilatory metal reduction in uranium-contaminated aquifer sediments, *Appl. Environ. Microb.*, *68*(5), 2300-2306.

Lovley, D. R., and E. J. P. Phillips (1987), Rapid Assay for Microbially Reducible Ferric Iron in Aquatic Sediments, *Appl. Environ. Microb.*, *53*(7), 1536-1540.

Minsley, B. J., J. Sogade, and F. D. Morgan (2007), Three dimensional self-potential inversion for subsurface DNAPL contaminant detection at the Savannah River Site, South Carolina, *Water Resour. Res.*, *43*(W04429), doi:10.1029/2005WR003996.

N'Guessan, A. L., H. A. Vrionis, C. T. Resch, P. E. Long, and D. R. Lovley (2008), Sustained Removal of Uranium From Contaminated Groundwater Following Stimulation of Dissimilatory Metal Reduction, *Environ. Sci. Technol.* , *42*(8), 2999-3004.

Naudet, V., A. Revil, J. Y. Bottero, and P. Begassat (2003), Relationship between self-potential (SP) signals and redox conditions in contaminated groundwater, *Geophys. Res. Lett.*, *30*(21), 2091.

Naudet, V., and A. Revil (2005), A sandbox experiment to investigate bacteria-mediated redox processes on self-potential signals, *Geophys. Res. Lett.*, *32*, L11405.

North, N. N., S. L. Dollhopf, L. Petrie, J. D. Istok, D. L. Balkwill, and J. E. Kostka (2004), Change in bacterial community structure during in situ Biostimulation of subsurface sediment cocontaminated with uranium and nitrate, *Appl. Environ. Microb.*, *70*(8), 4911-4920.

Nourbehecht, B. (1963), Irreversible Thermodynamic Effects in Inhomogenous Media and Their Applications in Certain Geoelectric Problems, 122 pp, Massachusetts Institute of Technology, Cambridge, Massachusetts.

Ntarlagiannis, D., E. A. Atekwana, E. A. Hill, and Y. Gorby (2007), Microbial nanowires: Is the subsurface "hardwired"?, *Geophys. Res. Lett.*, *34*(L17305)

Nyquist, J. E., and C. E. Corry (2002), Self-potential: The ugly duckling of environmental geophysics,, *Leading Edge of Geophysics*, *21*(5), 446-451.

Ortiz-Bernad, I., R. T. Anderson, H. A. Vrionis, and D. R. Lovley (2004), Resistance of solid-phase U(VI) to microbial reduction during in situ bioremediation of uranium-contaminated groundwater, *Appl. Environ. Microb.*, *70*(12), 7558-7560.

Peacock, A. D., Y. J. Chang, J. D. Istok, L. Krumholz, R. Geyer, B. Kinsall, D. Watson, K. L. Sublette, and D. C. White (2004), Utilization of microbial biofilms as monitors of bioremediation, *Microbial Ecol.*, *47*(3), 284-292.

Rabaey, K., K. Van de Sompel, L. Maignien, N. Boon, P. Aelterman, P. Clauwaert, L. De Schamphelaire, H. T. Pham, J. Vermeulen, M. Verhaege, P. Lens, and W. Verstraete

(2006), Microbial fuel cells for sulfide removal, *Environ. Sci. Technol.* , *40*(17), 5218-5224.

Reguera, G., K. D. McCarthy, T. Mehta, J. S. Nicoll, M. T. Tuominen, and D. R. Lovley (2005), Extracellular electron transfer via microbial nanowires, *Nature*, *435*(7045), 1098-1101.

Reguera, G., K. P. Nevin, J. S. Nicoll, S. F. Covalla, T. L. Woodard, and D. R. Lovley (2006), Biofilm and nanowire production leads to increased current in Geobacter sulfurreducens fuel cells, *Appl. Environ. Microb.*, *72*(11), 7345-7348.

Reimers, C. E., P. Girguis, H. A. S. III, L. M. Tender, N. Ryckelynck, and P. Whaling (2006), Microbial fuel cell energy from an ocean cold seep, *Geobiology*, *4*, 123-136.

Sato, M., and H. M. Mooney (1960), The electrochemical mechanism of sulfide self-potentials, *Geophysics*, *25*, 226-249.

Senko, J. M., J. D. Istok, J. M. Suflita, and L. R. Krumholz (2002), In-situ evidence for uranium immobilization and remobilization, *Environ. Sci. Technol.* , *36*(7), 1491-1496.

Slater, L., D. Ntarlagiannis, N. Yee, M. O'Brien, C. Zhang, and K. H. Williams (2008), Electrodic voltages in the presence of dissolved sulfide: Implications for monitoring natural microbial activity, *Geophysics*, *73*(2), F65-F70.

Tender, L. M., C. E. Reimers, H. A. Stecher, D. E. Holmes, D. R. Bond, D. A. Lowy, K. Pilobello, S. J. Fertig, and D. R. Lovley (2002), Harnessing microbially generated power on the seafloor, *Nat. Biotechnol.*, *20*(8), 821-825.

Vrionis, H. A., R. T. Anderson, I. Ortiz-Bernad, K. R. O'Neill, C. T. Resch, A. D. Peacock, R. Dayvault, D. C. White, P. E. Long, and D. R. Lovley (2005), Microbiological and geochemical heterogeneity in an in situ uranium bioremediation field site, *Appl. Environ. Microb.*, *71*(10), 6308-6318.

Williams, K. H., S. S. Hubbard, and J. F. Banfield (2007), Galvanic interpretation of self-potential signals associated with microbial sulfate-reduction, *J. Geophys. Res.* , *112*, G03019.

Wu, W. M., J. Carley, T. Gentry, M. A. Ginder-Vogel, M. Fienen, T. Mehlhorn, H. Yan, S. Caroll, M. N. Pace, J. Nyman, J. Luo, M. E. Gentile, M. W. Fields, R. F. Hickey, B. H. Gu, D. Watson, O. A. Cirpka, J. Z. Zhou, S. Fendorf, P. K. Kitanidis, P. M. Jardine, and C. S. Criddle (2006), Pilot-scale in situ bioremediation of uranium in a highly contaminated aquifer. 2. Reduction of U(VI) and geochemical control of U(VI) bioavailability, *Environ. Sci. Technol.*, *40*(12), 3986-3995.

Yabusaki, S. B., Y. Fang, P. E. Long, C. T. Resch, A. D. Peacock, J. Komlos, P. R. Jaffe, S. J. Morrison, R. D. Dayvault, D. C. White, and R. T. Anderson (2007), Uranium removal from groundwater via in situ biostimulation: Field-scale modeling of transport and biological processes, *J. Contam. Hydrol.*, *93*(1-4), 216-235.

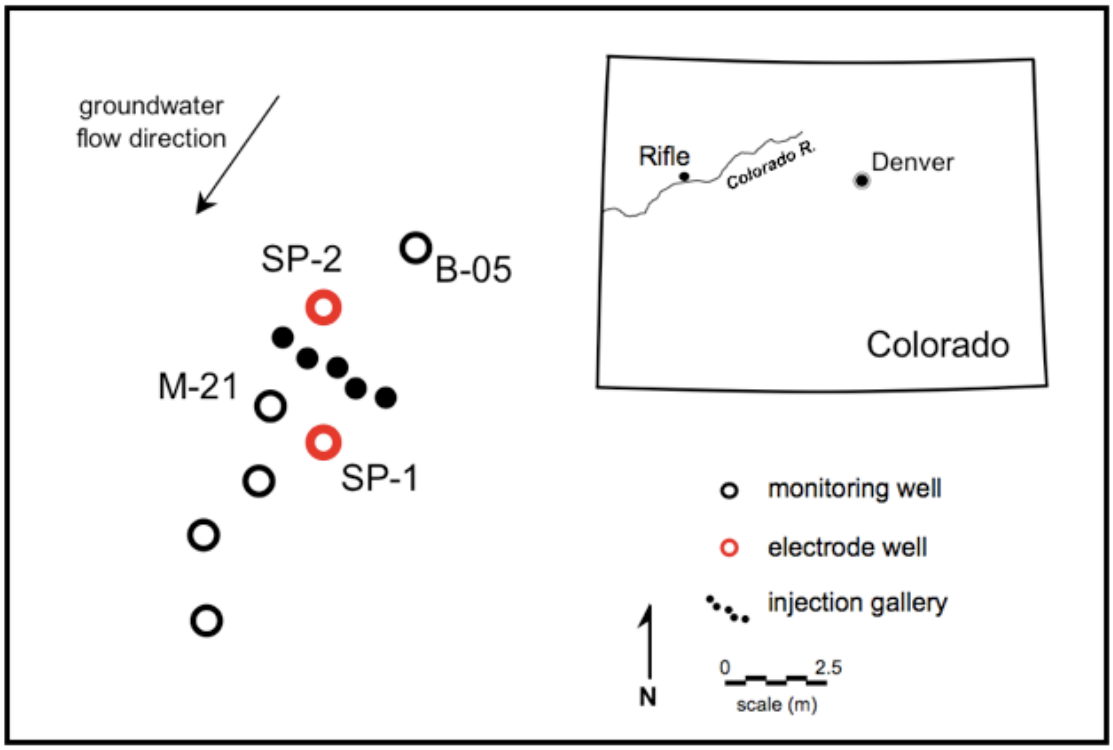

Figure 1. Plan map of the injection gallery and monitoring well locations used during the uranium bioremediation experiment near Rifle, Colorado (inset). Borehole electrodic potential data were acquired along wells SP-1 and SP-2, with the former located approximately 2.0 m downgradient of the injection gallery.

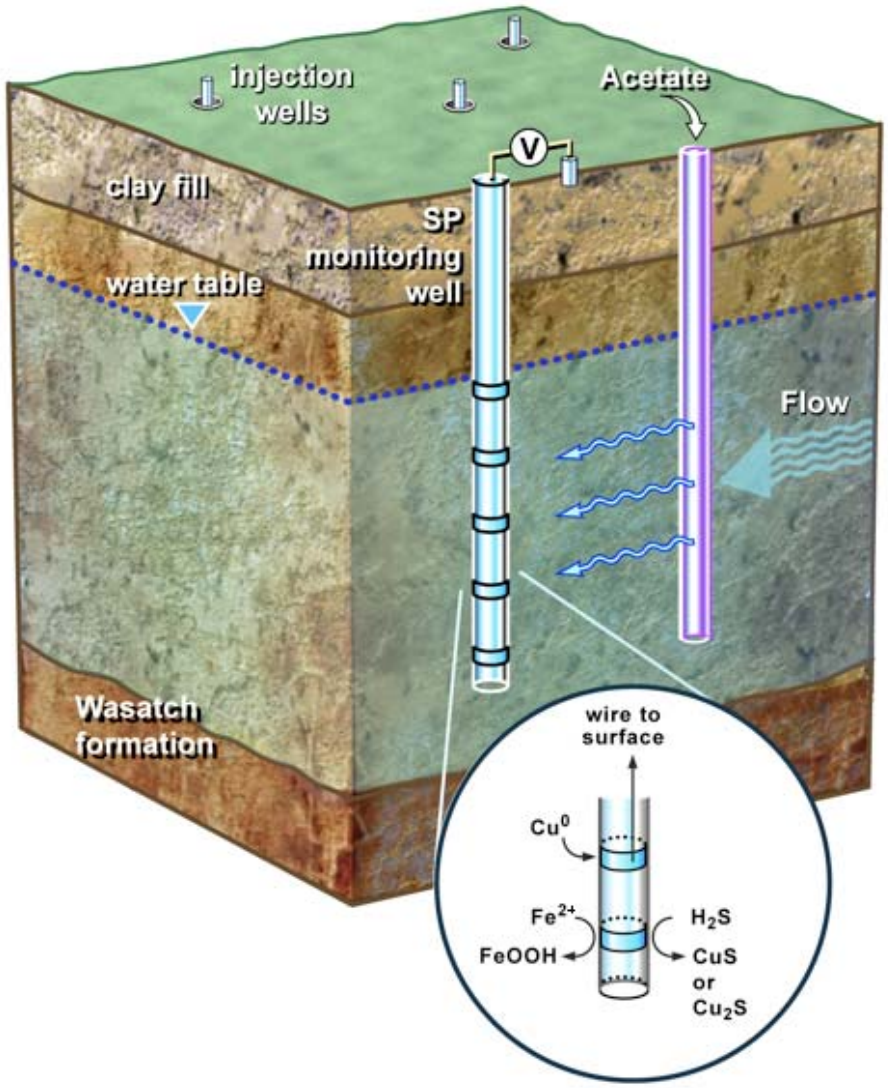

Figure 2. Schematic representation of the electrodic potential (EP) monitoring approach. Copper electrodes are affixed to the outside of well casings and used to monitor changes in geochemical conditions during stimulated microbial activity. A galvanic cell is completed upon connection of the subsurface electrodes and a surface-based reference (e.g. $Cu/CuSO_4$) through a high-impedance voltmeter. (Inset) Anodic reactions at the electrode surface are specific to sulfate (H_2S-mediated) and iron (Fe^{2+}-mediated) reduction, with measured voltages diagnostic of the predominant metabolic process.

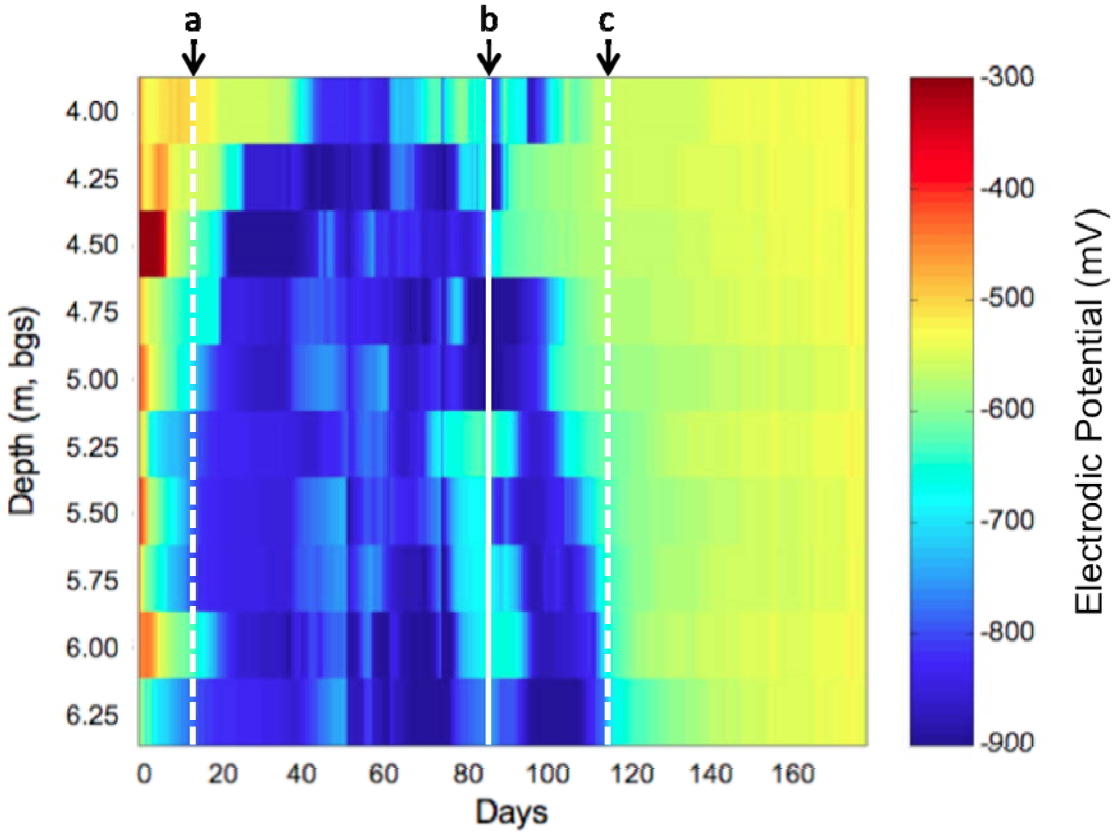

Figure 3. Electrodic potential data acquired along well SP-1. The depth to each measurement electrode and the time elapsed since the start of acetate injection are shown on the vertical and horizontal axes, respectively, with the color bar representing the magnitude of the electrodic potential signal. The potentials were diagnostic of stimulated sulfate reduction, with elevated sulfide concentrations present during the indicated interval ('a' to 'c'). Acetate injection was halted on day 68, with levels falling below detection by day 84 ('b').

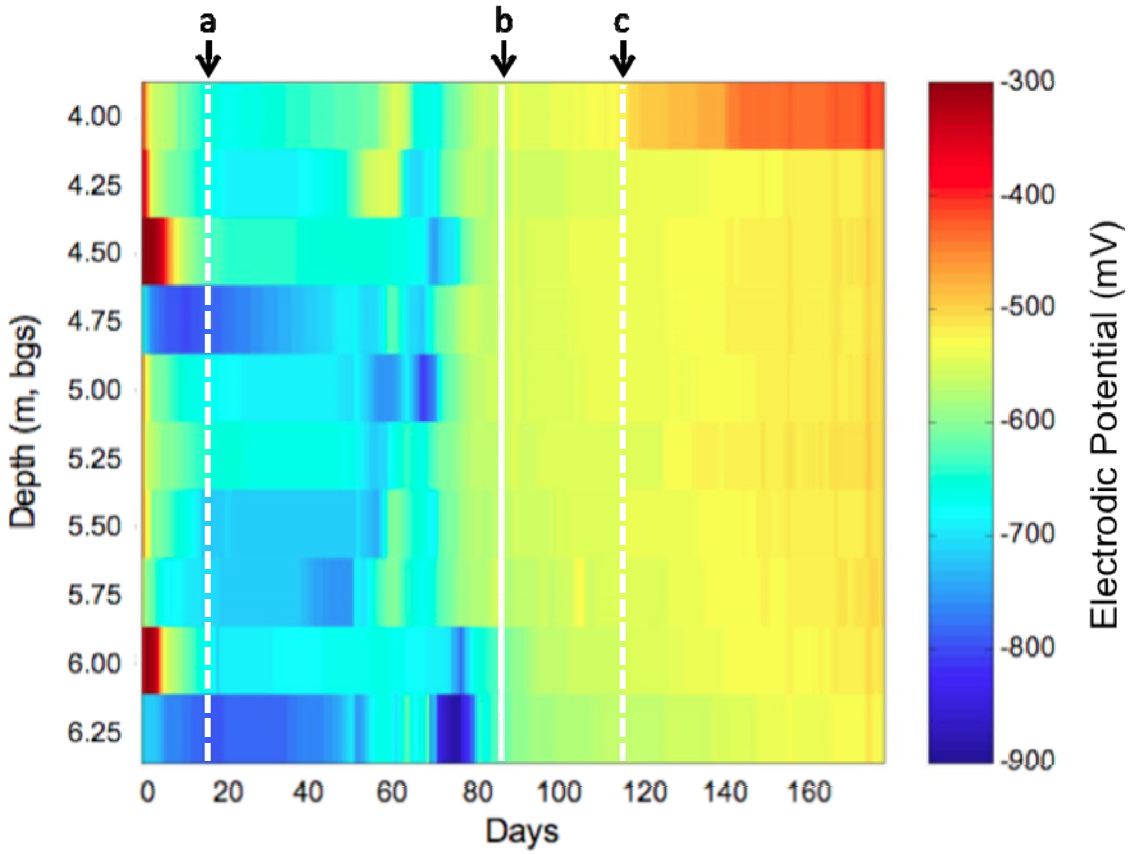

Figure 4. Electrodic potential data acquired along well SP-2, with axes, color scale, and labels (e.g. a, b, and c) identical to those shown in Figure 3.

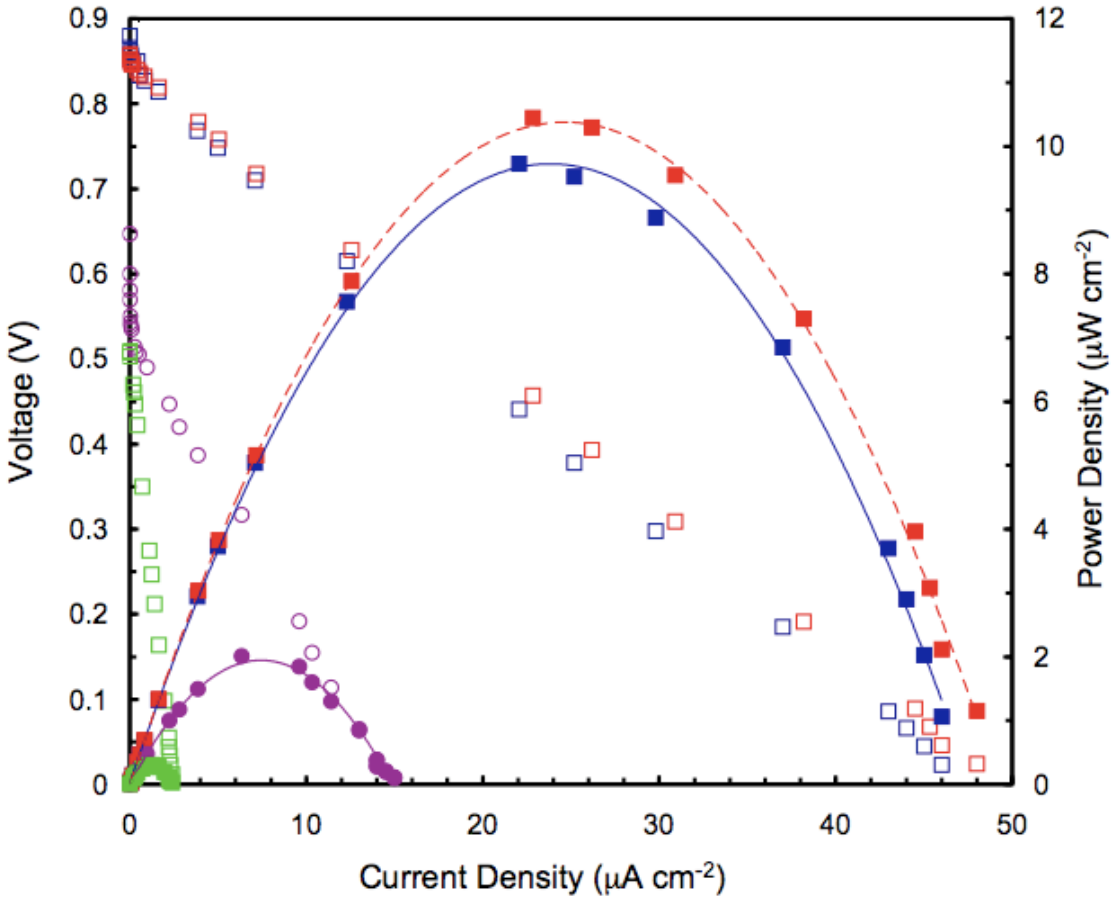

Figure 5. Current-voltage (open symbols) and current-power (closed symbols) relationships for the 6.5 m electrode depth in SP-1 (blue, red, and green) and SP-2 (purple). Data were obtained 58 (blue, purple), 85 (red) and 150 (green) days after beginning acetate addition. Current flow was determined by connecting the reference and measurement electrodes through a resistor of known value; total current flow and power production were then determined by iteratively lowering resistance of the circuit.

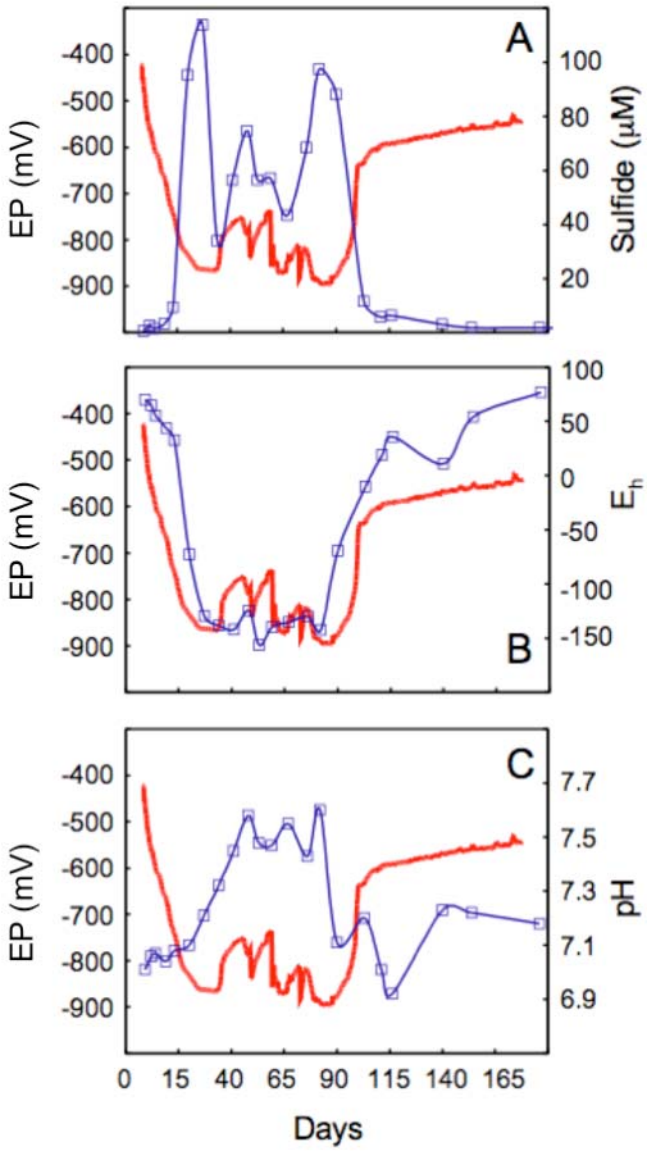

Figure 6. Temporal relationship between three key geochemical parameters "(sulfide, Eh, and pH) measured in well M-21 and the electrodic potential (EP) response of a discrete electrode located 5.0-m below ground surface in well SP-1 (red line). Variation in the EP response during the period of sulfate-reduction (15 to 100-days) is believed to result from differences in the dominant sulfide-mediated anodic half-cell reaction. Geochemical conditions that favor the stability of either CuS or Cu_2S will result in EP values that differ by approximately 180 mV (Figs. 7, S7).

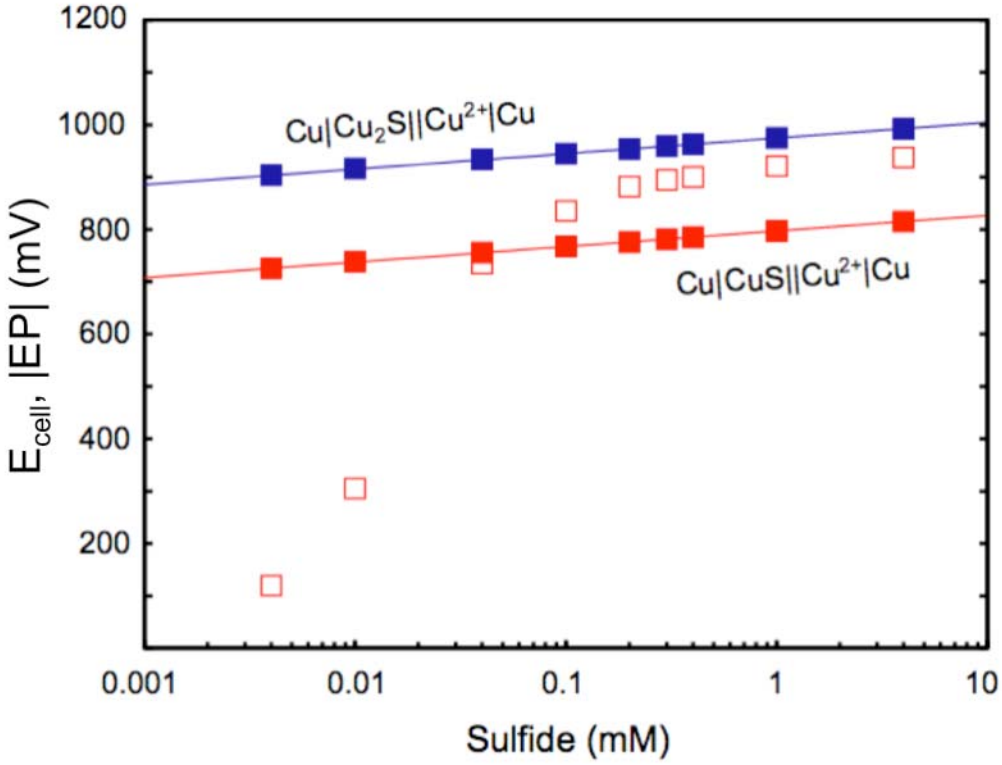

Figure 7. Electrodic potentials (EP) measured using a galvanic cell comprised of a $Cu/CuSO_4$ reference electrode (cathode; 1M $CuSO_4$) and a Cu^0 measurement electrode (anode) exposed to varying sulfide concentrations. Shown are the chalcocite (Cu_2S) and covellite (CuS) cell potentials as a function of $[S^{2-}]$ (bold lines), the measured EP values (absolute value; open squares) and theoretical cell potentials (closed squares) at nine discrete sulfide concentrations. The theoretical cell potentials were determined over the $[HS^-]$ range indicated at 25ºC and pH 7.5, as were the measured potentials.

Auxiliary Information. This following is auxiliary/supporting information consisting of eight figures intended to supplement the material presented in the manuscript. These include a photograph of the electrode-affixed well casings, co-plots of electrodic potential and geochemical data, an Eh-pH diagram for the Cu-S-O system, current-voltage/current-power relationships, and theoretical cell potentials for the Fe(II)/FeOOH||Cu(II)/Cu system.

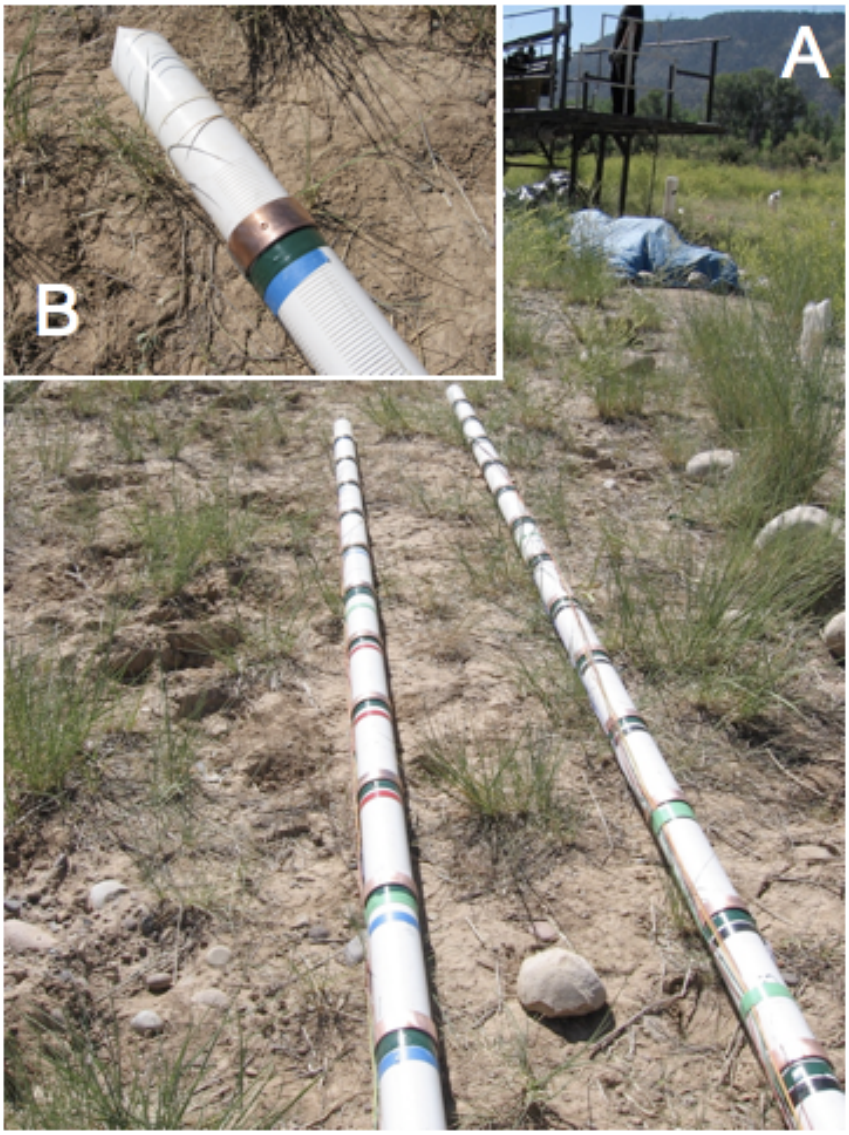

Figure S1. (A) Photograph of the electrode-modified casings; the metallic copper measurement electrodes were installed on the outside of the well casing at 0.25-m intervals with the reference electrode consisting of a $Cu/CuSO_4$ electrode at the ground surface (not shown). (B) Close-up view of the bottommost electrode used to obtain the current-voltage and current-power relationships.

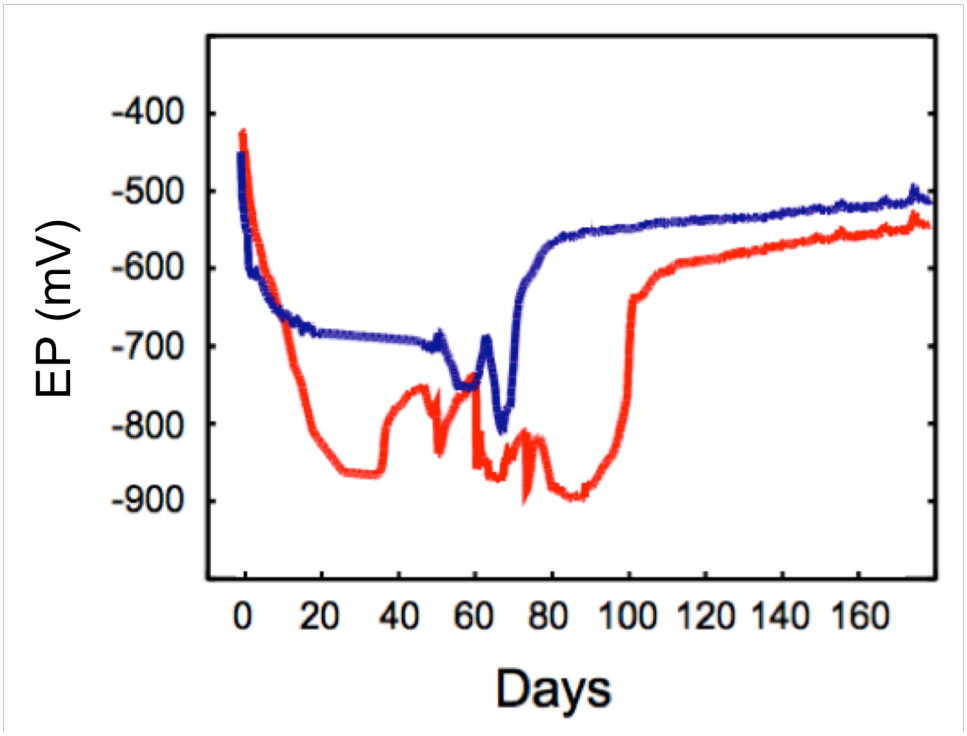

Figure S2. Electrodic potential (EP) data acquired for a discrete electrode depth (5.0 m) in wells SP-1 (red) and SP-2 (blue). The transition to relatively stable, post-amendment values was delayed in SP-1 by 31 days.

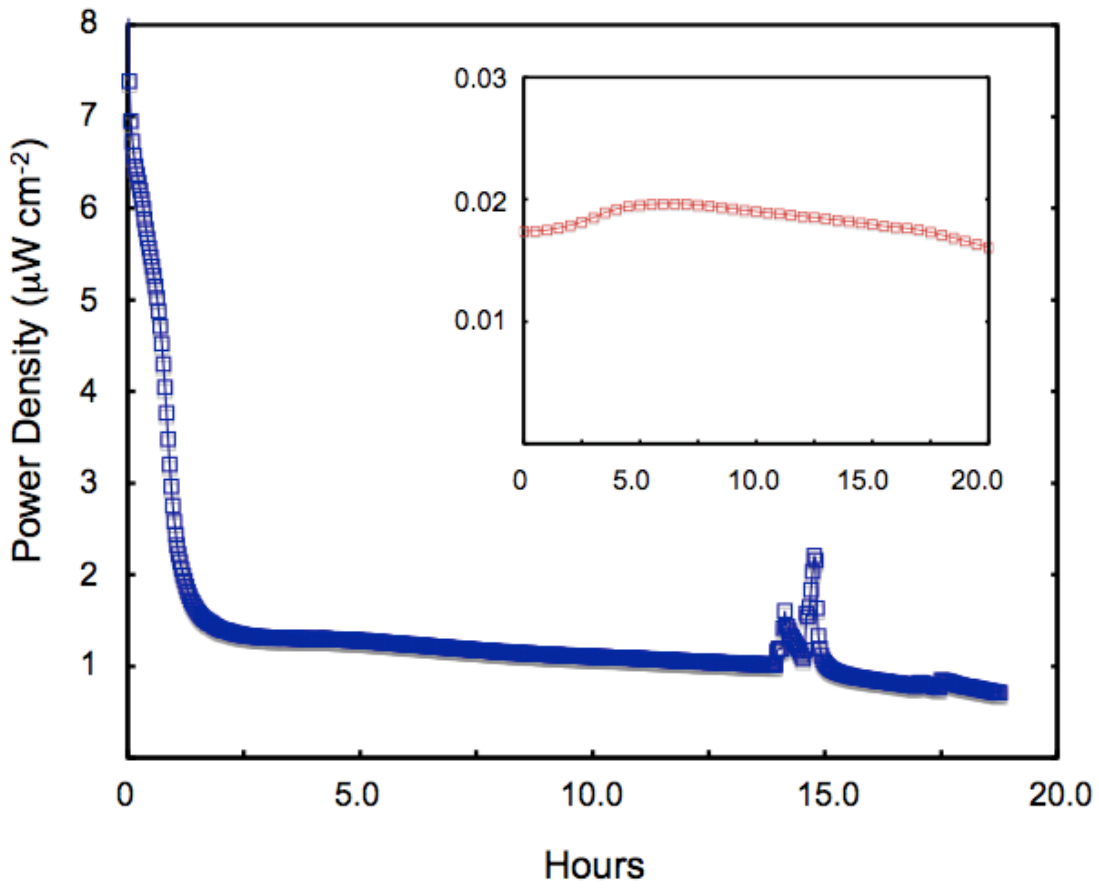

Figure S3. Temporal change in power density in SP-1 for the 6.5 m electrode depth 59 days after beginning acetate addition, as compared to pre-injection values (inset). Power production was monitored after connecting the borehole electrode to a surface based reference electrode through a 500-Ω resistor. Variability in the power density response after 14-hours corresponded to the repeated raising and lowering of an instrument within the wellbore.

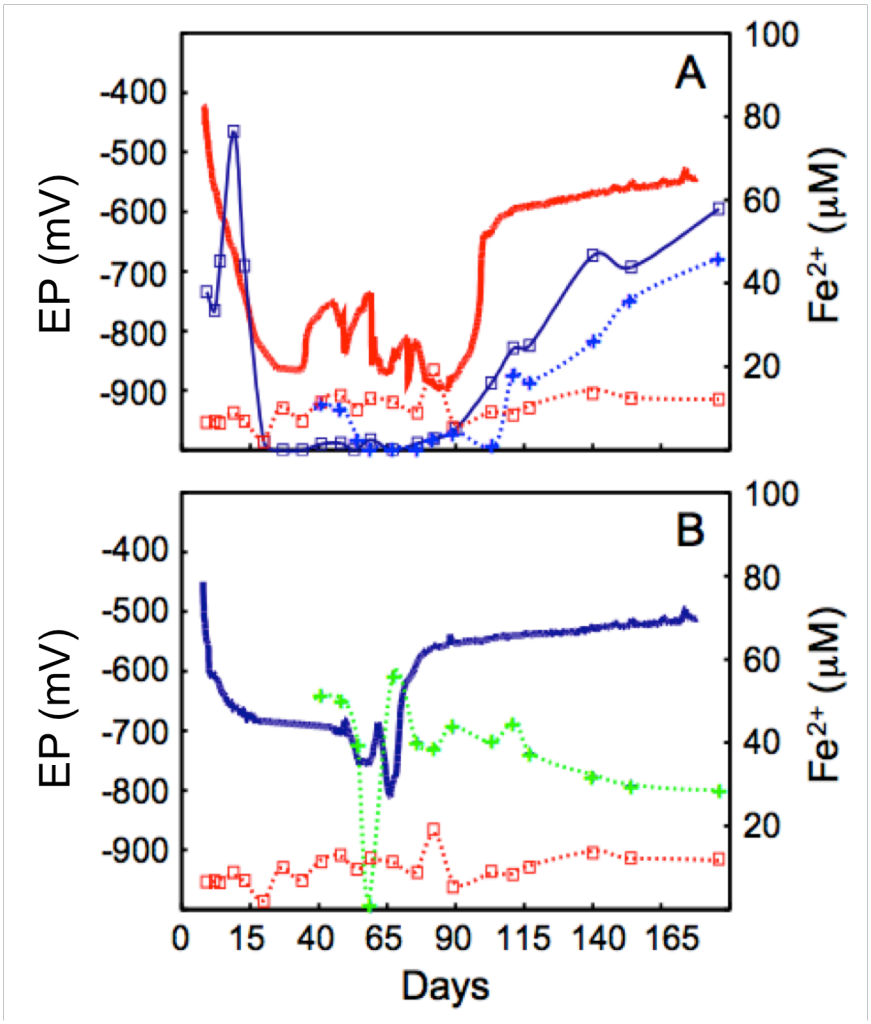

Figure S4. Temporal relationship between electrodic potential (EP) in SP-1 (A; red line) and SP-2 (B; blue line) and the ferrous iron concentration measured in M-21 (blue square), B-05 (red square), SP-1 (blue cross), and SP-2 (green cross). The large increase in ferrous iron measured in M-21 and SP-1 after 110 days correspond to the disappearance of both acetate and sulfide from groundwater.

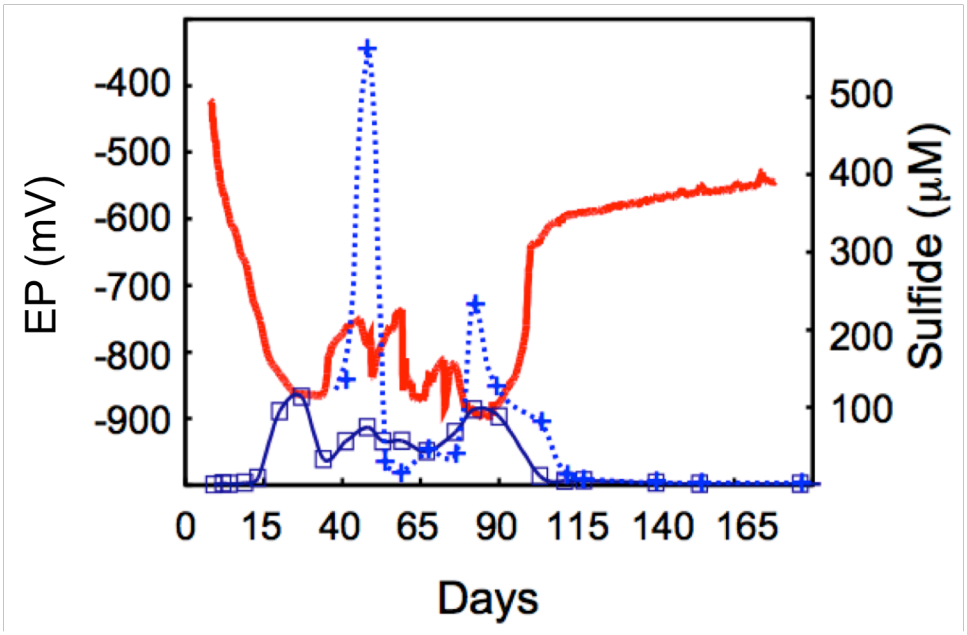

Figure S5. Temporal relationship between electrodic potential (EP) in SP-1 (red line) and the sulfide concentration measured in M-21 (blue square) and SP-1 (blue cross). Although sulfide concentrations were not measured in SP-1 prior to day 42, the trend in sulfide accumulation and disappearance is similar to, and typically in excess of, that measured in M-21, the nearest monitoring well.

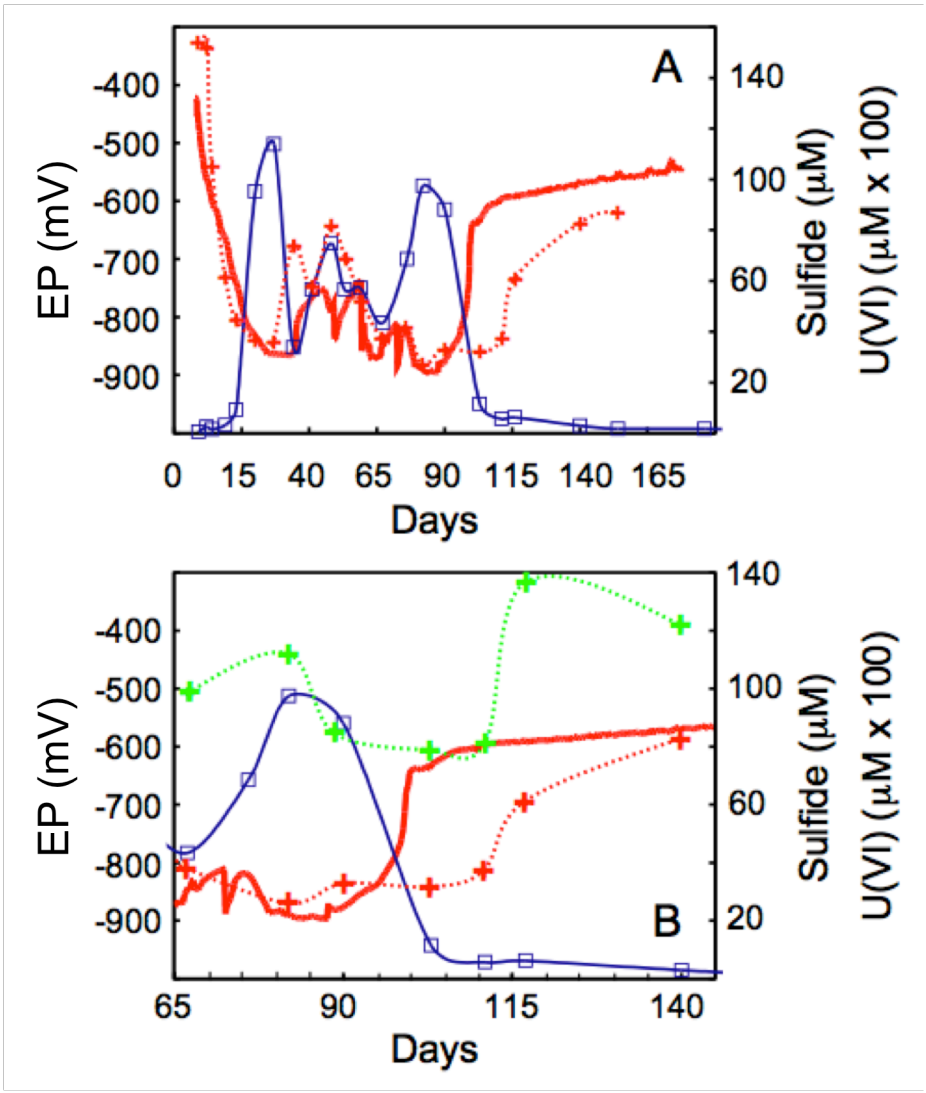

Figure S6. (A) Temporal relationship between electrodic potential (EP) in SP-1 (red line) and sulfide (blue square) and uranium (red cross) concentrations measured in M-21. (B) Expanded view of the time interval immediately following cessation of acetate addition. Within 12 days following the rebound in voltages, uranium concentrations in the downgradient wells began to increase. For comparison, the change in the upgradient uranium concentration measured in B-05 (green cross) is shown.

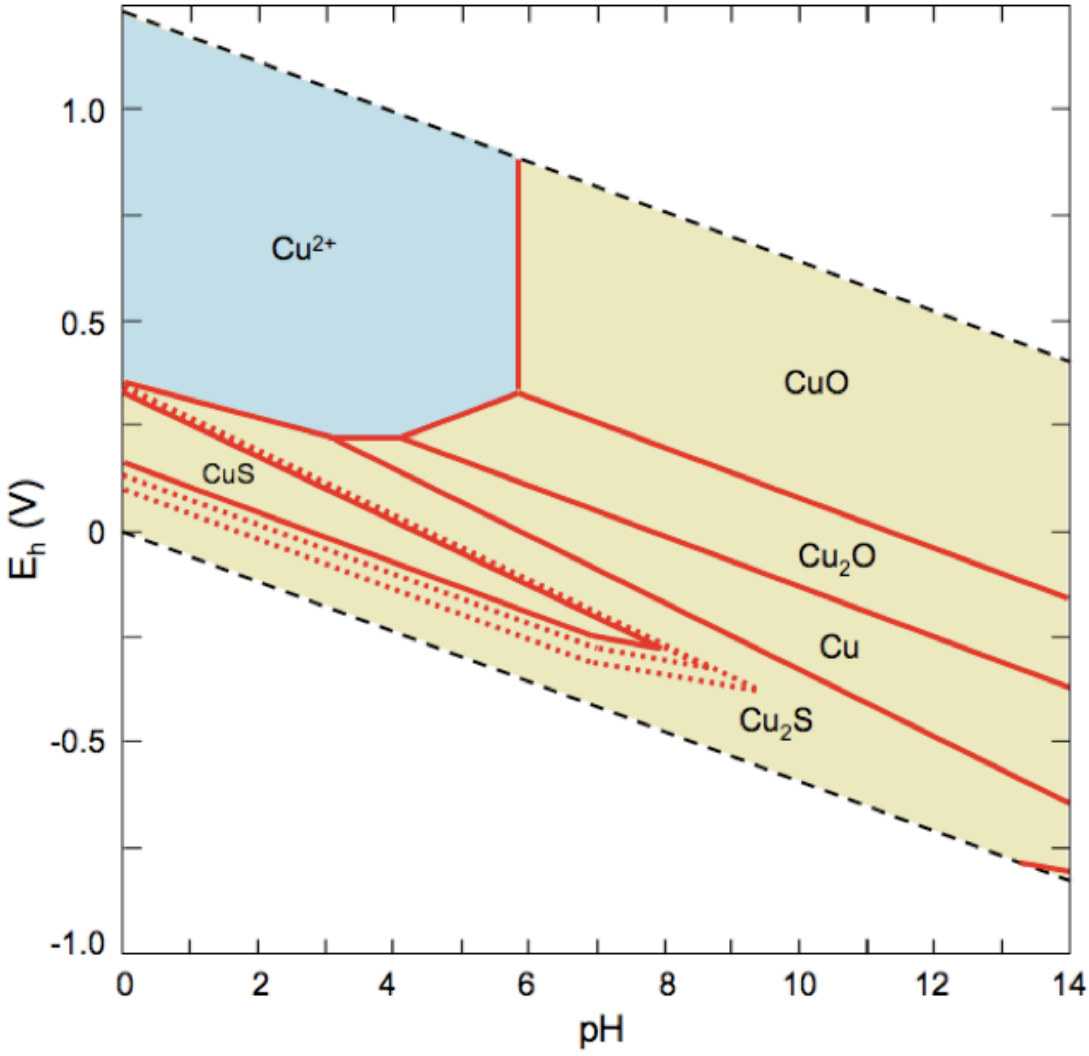

Figure S7. Eh-pH diagram for the Cu-S-O system. Expansion of the covellite (CuS) stability field into that for chalcocite (Cu_2S) occurs as the sulfide concentration increases; three sulfide concentrations (0.01, 0.1, and 1 mM) are plotted, with the lowest concentration indicated by the bold border. Temporal variations in sulfide concentration, pH, and Eh during the biostimulation experiment would be expected to favor a specific copper sulfide phase, thereby influencing the cell potential and measured EP response.

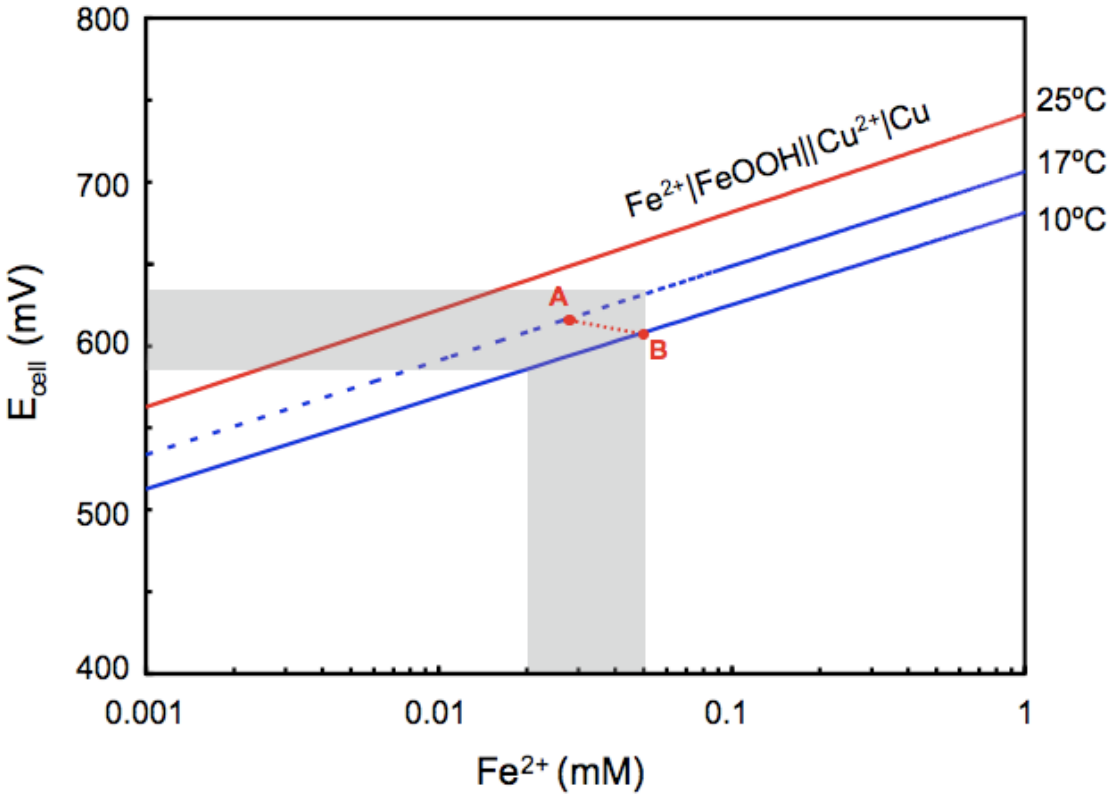

Figure S8. Theoretical cell potentials for the coupled anodic Fe(II)/Fe(III) and cathodic C(II)/Cu(0) half-cells as function of ferrous iron concentration and temperature at pH 7. Fe(II)-dependent potentials may be expected in the absence of dissolved sulfide, with the predicted values in excellent agreement with those observed after 100-days (Fig. 9) for the range of iron concentrations highlighted (grey region). As indicated in moving from 'A' to 'B', a decrease in the observed SP voltage would be expected as temperatures decrease, even under conditions where ferrous iron concentrations increase.